Geophysical Research Letters

RESEARCH LETTER
10.1029/2020GL088171

Mid-Holocene Sahara-Sahel Precipitation From the Vantage of Present-Day Climate

Peter Molnar[1,2] and **Balaji Rajagopalan**[2,3]

[1]Department of Geological Sciences, University of Colorado Boulder, Boulder, CO, USA, [2]Cooperative Institute for Research in Environmental Sciences, University of Colorado Boulder, Boulder, CO, USA, [3]Department of Civil Environmental and Architectural Engineering, University of Colorado Boulder, Boulder, CO, USA

Key Points:
- More than half of paleoclimatic estimates of Mid-Holocene Sahara-Sahel rainfall can be explained by four large-scale forcings
- These forcings are ENSO, AMO, hemispherical temperature difference, and the net energy input at the equator
- We obtained ~2.5° northward shifts of latitude bands along which rainfall today averages 1,000, 500, or 200 mm/year

Correspondence to:
B. Rajagopalan,
balajir@colorado.edu

Citation:
Molnar, P., & Rajagopalan, B. (2020). Mid-Holocene Sahara-Sahel precipitation from the vantage of present-day climate. *Geophysical Research Letters*, *47*, e2020GL088171. https://doi.org/10.1029/2020GL088171

Received 3 APR 2020
Accepted 23 JUN 2020
Accepted article online 8 JUL 2020

Abstract To account for the wet mid-Holocene (ca. 6 ka) Sahara-Sahel region, we exploit teleconnections from four large-scale ocean-atmosphere-land forcings: El Niño–Southern Oscillation (ENSO), Atlantic Multidecadal Oscillation (AMO), hemispherical temperature difference, and net energy input at the equator; they offer theoretical bases for estimating effects of large-scale forcing on mid-Holocene Sahara-Sahel rainfall. Together, these forcings explain 16–64% of historical rainfall variability, with the highest percentages in the Sahel region. With estimates for mid-Holocene time, latitudes where rainfall today averages 1,000, 500, or 200 mm/year are reconstructed to have lain ~2.5° farther north. Calculated mid-Holocene rainfall at 15°N, 17.5°N, and 20°N exceeds that today by ~250, 100, and 20 mm/year. These shifts account for more than half of paleoclimatic estimates of mid-Holocene rainfall and are comparable with the General Circulation Model (GCM) runs that match paleorainfall estimates most closely. Mid-Holocene radiation may have affected Sahel precipitation indirectly via teleconnections from oceanic regions.

1. Introduction

Rainfall in northern Africa occurs in an east-west band with a boundary, ~5° in width, separating a band with 1,000 mm/year near ~10°N from where rainfall is less than 100 mm/year (Figure 1). Paleoclimatic evidence shows that this band lay 300–500 km farther north in mid-Holocene time, at 6 ka (6,000 years ago). Simple logic buttressed by numerical calculations (e.g., Kutzbach, 1981) suggests that the more intense summer insolation at 6 ka than today should lead to wetter Northern Hemisphere subtropics than today. General Circulation Model (GCM) simulations (e.g., Braconnot et al., 2000, 2002, 2007a, 2007b, 2012; de Noblet et al., 1996; Harrison et al., 1998, 2014, 2015; Joussaume et al., 1999; Kageyama et al., 2013; Marzin & Braconnot, 2009; Otto-Bliesner et al., 2006; Perez-Sanz et al., 2014), however, commonly fail to match the paleoclimatic evidence for an ~300- to 500-km northward displacement of the rainfall belt. Accordingly, the wet mid-Holocene Sahel has challenged climate dynamicists for decades.

In fact, there are two challenges. First, which parameters should modelers tune, and how should they be tuned to bring simulations into accord with the paleoclimatic data? Second, how does summer insolation at 6 ka create a wetter Sahel than today? We address this latter question using the Earth's present-day climate as a template and basic theory as justification for its use. We examine the possibility that mid-Holocene insolation affected Sahel rainfall more via teleconnections than from direct, enhanced summer insolation over the Sahel itself. We rely on teleconnections known to affect seasonal variations in rainfall over northern Africa and appropriate differences between present-day and mid-Holocene climates to scale those teleconnections.

For present-day precipitation, the standard against which we compare mid-Holocene rainfall (Figure 1), we used monthly rainfall on a 0.5° × 0.5° grid for 1951–2016 from Climate Research Unit (CRU) of University of East Anglia (Harris et al., 2014). Because the El Niño cycle spans the period from May to April, we computed the annual average rainfall for that period.

2. Paleoclimate Evidence for a Wetter Mid-Holocene Than Present-Day Sahel

Two classes of observations suggest a wetter 6-ka Sahel: widespread lake deposits and paleobotanical evidence of plants living in regions where desert conditions prohibit them today. Summaries of

10.1029/2020GL088171

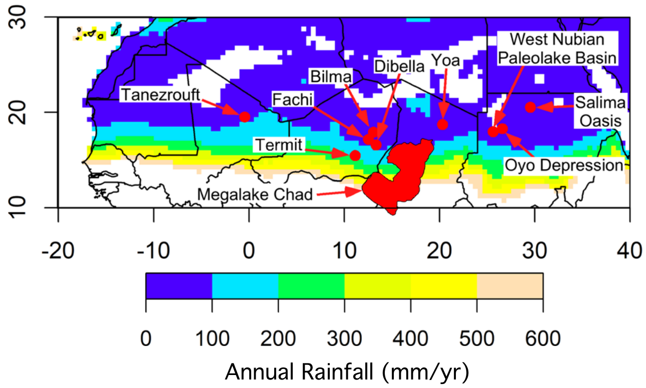

Figure 1. Map of northern Africa showing summer rainfall today, with sites where paleoclimate data constrain past rainfall amounts. Mid-Holocene lake levels were higher than today at many lakes: Tanezrouft, Bilma, Fachi, Dibella, Termit, one near 20.3°N, 0.7°W, another at 20°30–21°N; 0–1°W, Lake Megachad, ~12–17°N, 13–18°E, Lake Yoa, another near 18.5°N, 25.5°E), and the west Nubian paleolake basin (e.g., Gasse & Roberts, 2005; Gasse & Van Campo, 1994; Hillaire-Marcel et al., 1983; Hoelzmann et al., 2000; Petit-Maire & Riser, 1981). Elsewhere, especially farther east in the Salima Oasis and the Oyo Depression, pollen shows wetter climates than today (e.g., Haynes et al., 1989; Ritchie et al., 1985; Ritchie & Haynes, 1987).

mid-Holocene lakes in Africa (Figure 1) call for perennial lakes in regions where today water accumulates rarely (Gasse & Roberts, 2005; McGee & deMenocal, 2017; Quade et al., 2018; Street & Grove, 1976). Gasse and Van Campo (1994) reported more water at 6 ka than today in paleolakes Bilma, Fachi, Dibella, and Termit. Hillaire-Marcel et al. (1983) reported early Holocene lakes near 20.3°N, 0.7°W in Mali that then dried up between 6.5 and 5.5 ka. Petit-Maire and Riser (1981) reported Holocene lacustrine deposits with fish fossils at Tanezrouft, and to sustain a lake, they inferred that the Sahel belt lay 3–4° north of its present latitude.

Quantitative estimates of precipitation rates based on lake depths and areas also call for a northward displacement of the rain belt. For Megalake Chad, ~12–17°N, 13–18°E, where the current rainfall is 350 mm/year, Kutzbach (1980) inferred greater than 650 mm/year between 10,000 and 5,000 ka, 300–350 mm/year greater than present day (Hoelzmann et al., 1998). At Lake Yoa, Kröpelin et al. (2008) reported a drop from ~250 mm/year at 6 ka to <150 mm by 4.3 ka, where today it is <50 mm/year. For a paleolake farther east, near 18.5°N, 25.5°E, Hoelzmann et al. (2000) estimated annual rainfall of at least 350 mm, probably 500 mm, and if the lake were very large, 1,100 mm, compared to 15 mm today. Abell and Hoelzmann (2000) inferred maximum wetness at about 9 ka and marked drying after ~5,600 ka. Maybe we should assume an amount close to 350–500 mm at 6 ka. In a summary, Quade et al. (2018) considered it likely that only Lake Chad occupied areas as large as ~5,000 km^2; they argued that many estimates of past annual rainfall amounts have been overestimated.

Similarly, differences in vegetation call for more mid-Holocene than present-day rainfall (e.g., Haynes et al., 1989; Jolly et al., 1998; Lézine et al., 2011; Peyron et al., 2006; Tierney et al., 2017). Most call for 400- to 500-km northward displacements of vegetation and hence of rain bands (e.g., Abell & Hoelzmann, 2000; Lézine & Casanova, 1989; Mees et al., 1991; Pachur & Hoelzmann, 1991; Pachur & Kröpelin, 1987; Ritchie et al., 1985; Ritchie & Haynes, 1987). In a synthesis of Holocene paleoanthropology and paleoarcheology, Kuper and Kröpelin (2006) inferred contours of rainfall for the Sudan region for 7–5.3 ka. They showed the 150-, 300-, and 450-mm contours just south of 22°N, ~18.5°N, and near ~17°N, respectively. Today, all lie south of ~15°N (Figure 1). Collectively, these data suggest that the latitude band with 200–300 mm/year today lay 300–500 km farther north in mid-Holocene time.

3. Mid-Holocene Sahel Precipitation Simulated Using GCMs

Although the past decades have seen increasingly closer matches of simulated rainfall over the Sahel to that inferred from paleoclimate data, models that were tuned to match those data have continued to fall short in both precipitation amounts and latitudes of the rain belt. Coupled atmosphere-ocean GCMs do better than those that use a slab ocean (e.g., Alder & Hostetler, 2015; Bosmans et al., 2012; Braconnot et al., 2000, 2002, 2007a, 2007b, 2019; Brown et al., 2008; Dallmeyer et al., 2018; Liu et al., 2017; Otto, Raddatz, Claussen, Brovkin, & Gayler, 2009; Otto, Raddatz, & Claussen, 2009; Shin et al., 2006). In particular, using an atmospheric GCM and 6-ka insolation, Braconnot et al. (2000) simulated the rain belt to lie ~2° north of that today, but with a coupled GCM, 3° north of it, if still short of some mid-Holocene estimates that reach 5°. Perhaps as impressive, however, are differences among modeled Sahel rainfall. Braconnot et al. (2007a) reported simulated differences between 6-ka and present-day rainfall over the Sahel ranging from 0.2 to 1.6 mm/day, and Dallmeyer et al. (2015) reported a range of 0.5 to 3.5 mm/day. Differences among simulations span factors as high as 8 (Braconnot et al., 2007a) and 7 (Dallmeyer et al., 2015). Harrison et al. (2015) concluded in a recent synthesis that attempts using paleosimulations to constrain climate sensitivity have been disappointing.

Efforts to bring GCM simulations of rainfall into accord with paleoclimatic evidence have exploited a greener Sahel and Sahara than today. In addressing the twentieth century southward migration of the rain belt and the aridification of the Sahel, Charney (1975) showed that an increase in albedo, resulting from the replacement of a green absorbing surface by reflective desert, could lead to a southward migration of the rain belt. Others have exploited the converse and shown how a greener Sahel would reduce albedo and move the rain belt northward (e.g., Bonfils et al., 2001; Boos & Korty, 2016; Braconnot et al., 2007b, 2019; Kutzbach et al., 1996; Levis et al., 2004; Pausata et al., 2016; Su & Neelin, 2005; Swann et al., 2014), in some cases with additional feedbacks, like reduced advection of cool, dry air (with low moist static energy) into the region (Su & Neelin, 2005) and even a greener Eurasia (Swann et al., 2014). Most assessments of the roles of different albedo and different evapotranspiration between a green surface and desert show a much more important albedo (e.g., Kutzbach et al., 1996; Levis et al., 2004).

Differences in albedo may also explain differences among GCM simulations of rainfall. Levine and Boos (2017) showed that among 47 GCM simulations, mean values of summer albedo over the Sahel and Sahara span ~0.35–0.5, with standard deviations of ~0.6–0.12. Such standard deviations require differences of several tens of W/m^2 in insolation, compared with ~20 W/m^2 greater mid-Holocene than present-day summer insolation over the Sahel. Given the importance of albedo in accounting for the mid Holocene wet Sahel/Sahara, and large variations in assumed values for it, differences among simulated precipitation amounts among the GCMs ought not to be surprising.

4. Sea Surface Temperatures and Rainfall Over the Sahel

Sahel rainfall correlates with sea surface temperatures (SSTs) in a number of regions (e.g., Folland et al., 1986). Higher than normal Sahel rainfall corresponds with a cooler than normal tropical Pacific Ocean, during La Niña events (e.g., Giannini et al., 2003, 2008; Parhi et al., 2016; Pomposi et al., 2016, 2020; Shin et al., 2006). Giannini et al. (2008) noted that during the growth phases of warm El Niño episodes, the small Coriolis parameter allows the entire tropics to warm, and this warming stabilizes the tropical atmosphere against convection and inhibits rainfall (Chiang & Sobel, 2002). When the tropical Pacific is cool, cooler tropics elsewhere facilitate convection of a moist troposphere and lead to a wetter Sahel. To quantify tropical Pacific SSTs, we use the NINO3.4 index (average SSTs over 5°N to 5°S, 170–120°W).

A cool North Atlantic SST correlates with low rainfall in the Sahel (e.g., Biasutti & Giannini, 2006; Chiang & Friedman, 2012; Giannini et al., 2013; Kushnir & Stein, 2010; Liu et al., 2014; Marzin et al., 2013), though some emphasize tropical North Atlantic SSTs and others middle- or high-latitude North Atlantic SSTs (e.g., Biasutti et al., 2008; Giannini et al., 2003, 2008; Lu & Delworth, 2005). Liu et al. (2014) pointed out that a cool North Atlantic leads to strong westerly winds that advect cool air over North Africa. Although the link between that cool air, with low moist static energy, and the African monsoon requires consideration of radiation balance (Liu et al., 2014), in simple terms the advection of air with low moist static energy suppresses moist convection (Su & Neelin, 2005).

The North Atlantic Oscillation (NAO), a dominant phenomenon during winter, is linked with SST variability in the tropical Atlantic (e.g., Rajagopalan et al., 1998). Low frequency variability, quantified by the Atlantic Multidecadal Oscillation (AMO) (Enfield et al., 2001; Knight et al., 2005; Sutton & Hodson, 2005), modulates multidecadal rainfall variability over the Sahel and India (Zhang & Delworth, 2006). The AMO also correlates with the NAO and associated SST patterns (Peings & Magnusdottir, 2015). Thus, we chose the AMO index, the average SST over 0–80°N in the Atlantic Ocean (Trenberth & Shea, 2006), to quantify Atlantic Ocean SST variability for paleoclimate comparisons. The NINO3.4 and AMO indices are calculated using the Kaplan Extended v2 SST (Kaplan et al., 1998).

Summer Sahel precipitation correlates with the difference between SSTs in the Southern and Northern Hemispheres (e.g., Chiang & Friedman, 2012; Folland et al., 1986). Folland et al. (1986) calculated a correlation coefficient of 0.72 between Sahel rainfall and that difference for the period 1901–1984. To capture the overall strength of the hemispherical temperature gradient, we computed the annual (May–April) mean temperature difference based on land and SSTs, HadCRUT4 (Morice et al., 2012).

Finally, Bischoff and Schneider (2014, 2016) and Schneider et al. (2014) showed that the ratio of two quantities determines the latitude of the energy flux equator (EFE), where convergence from the two hemispheres is maximum and hence near the Intertropical Convergence Zone (ITCZ) where rainfall commonly is maximum. Those two quantities comprise the flux of energy across the equator, and the net energy input at the equator, with the EFE moving poleward with increasing flux across the equator and remaining close

10.1029/2020GL088171

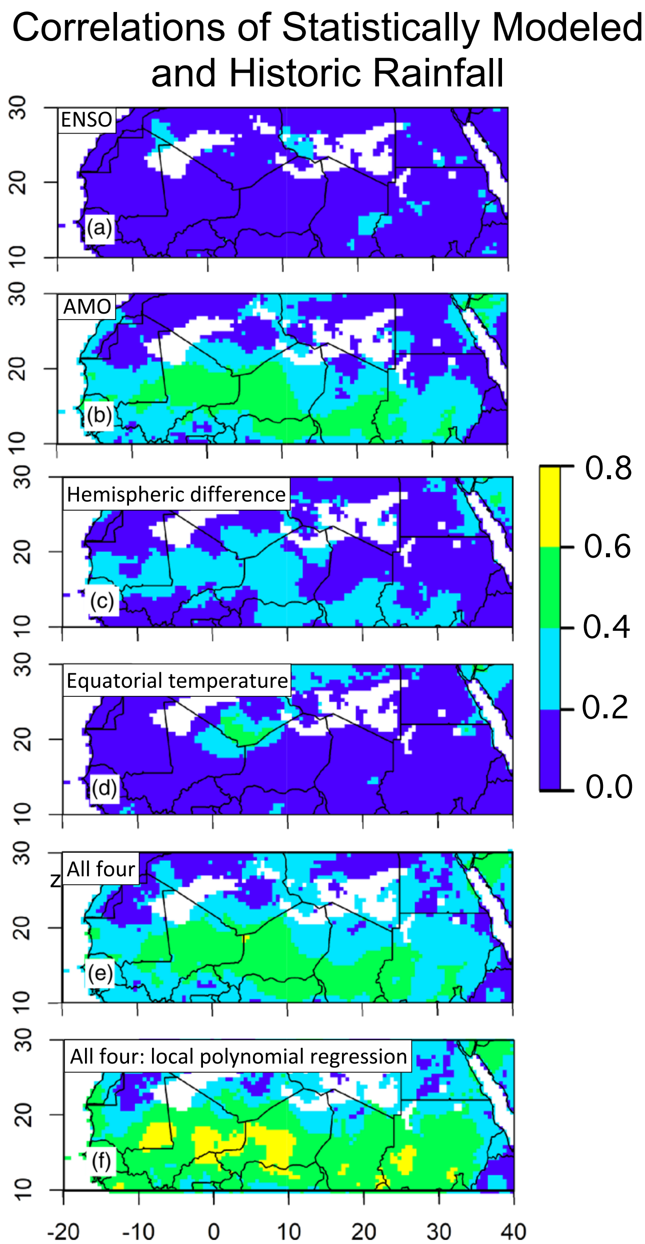

Figure 2. Correlation maps of historical annual rainfall over northern Africa with estimates based on regression models of that rainfall at each grid point, for the period 1951–2016: Linear regressions (a) with NINO34 index, (b) with AMO index, (c) with hemispherical temperature gradient index, (d) with surface temperatures from the HadCRUT4 data set between 5°S and 5°N and south of the Sahel, between 20°W and 49°E, a surrogate for net energy input at the equator, and multiple linear regression (e) and local polynomial multiple regression (f) with all four indices.

to it with high energy input there. Globally averaged positions of the ITCZ and EFE match one another closely (Adam et al., 2016a), but in the African region, where both lie far from the equator in the summer rainy season, they differ by ~5° (Adam et al., 2016b). Adam et al. (2019) showed that interannual variability in GCM runs aimed at Holocene Sahel precipitation corroborated such a scaling. Although globally, shifts in the ITCZ must be small because of compensating heat transport by the ocean in the opposite direction (Donohoe et al., 2013; Green et al., 2019; Green & Marshall, 2017; Marshall et al., 2014; McGee et al., 2014), locally over continental regions shifts can be large. Accordingly, a warm Northern Hemisphere should draw the ITCZ northward into Africa and enhance rainfall over the Sahel, especially if the equatorial band does not heat abnormally rapidly (Adam et al., 2016b, 2019).

Given difficulties in estimating energy fluxes for paleoclimate time, we treat the hemispheric difference in surface temperatures as a proxy for cross equatorial energy fluxes (e.g., Green et al., 2017; Kang et al., 2008, 2009) and surface temperatures from the HadCRUT4 data set between 5°S and 5°N and south of the Sahel, between 20°W and 49°E, as a surrogate for net energy input at the equator. This latter assumption gains support from the correlation of net energy input with SSTs in the tropics (Adam et al., 2018, Figure 10).

The preponderance of evidence based on the past research surveyed above indicates that teleconnections from four large-scale forcings—ENSO, AMO, hemispherical temperature difference, and the energy flux at the equator—affect Sahel rainfall at multidecadal time scales. Moreover, because the role of each rests on a theoretical and sensible foundation, combining them to model Sahel rainfall does not depend merely on correlations.

Boos and Korty (2016) showed how zonal differences in energy flux affect Sahel precipitation. An unfortunate shortcoming in our study is an inablilty to quantify this for past climates.

To quantify the relationship of these teleconnections to Sahel rainfall variability, we first fit linear regressions between annual indices of the four forcings and annual rainfall for the period 1951–2016, at each grid point over Sahel region, 10–30°N; 20°W to 40°E (Figure 2). The ENSO (Figure 2a) correlation of ~0.2 over the entire region indicates that ENSO captures ~4% of rainfall variance. The AMO regression (Figure 2b) captures 16–36% of rainfall variance in the core Sahel region (12–17°N; 10°W to 20°E). This is consistent with strong multidecadal correlation between Atlantic SSTs and Sahel rainfall in previous studies and specifically between the AMO and rainfall in Martin et al. (2014). Outside of the core region, the regression captures 4–16% of variance and ~4% or less in the northern and eastern edges of the domain. The hemispherical temperature difference (Figure 2c) captures 4–16% of rainfall variance in the core region and ~4% in the rest. The equatorial temperature, like ENSO, captures ~4% of rainfall variance, though here the correlation is negative, as theory predicts (Figure 2d). The combination of these four indices in a multiple linear regression (Figure 2e) captures 4–36% of rainfall variance over almost the entire domain, except for small patches at the northern and eastern edges.

We recognize that Sahel rainfall may scale nonlinearly with the indices. To capture this nonlinearity, we performed a local polynomial regression (Loader, 1999). For a selected year, we fitted a linear regression to a subset of K nearest neighbors of each index, using a weighted least squares method, in which higher weights are assigned to nearest neighbors of the year in question, and least to the farthest. This is repeated for each year and at all grid points. We set the number of nearest neighbors, *K*, to the default 75% of the total number of 66 years of historical data. The local polynomial regression (Figure 2f) captures 36–64% of rainfall variance—over 12–17°N, 10°W to 10°E, 6–36% over the core Sahel region, and 4–16% over most of the rest of the domain. Thus, four large-scale forcings can parsimoniously model a significant portion (16–64%) of multidecadal rainfall variability over the Sahel region. We use the regression parameters from the local polynomial regression to reconstruct Mid-Holocene Sahel rainfall.

5. Holocene SSTs and Predicted Rainfall in the Sahel

Abundant paleoceanographic evidence from eastern tropical Pacific suggests lower SSTs in that region at 6 ka (e.g., Koutavas et al., 2006; Koutavas & Sachs, 2008). Gill et al. (2016) synthesized such data to infer that SSTs in the NINO3.4 region, were 0.75°C cooler than today. Moreover, modern coupled ocean-atmospheric GCM runs commonly show reduced ENSO variance and a cooler Holocene than present-day equatorial Pacific. Saint-Lu et al. (2019) simulated a mid-Holocene equatorial Pacific SST distribution that differs little from what Gill et al. (2016) inferred.

Explanations for the Mid-Holocene La Niña-like state at 6 ka rely on perihelion at 6 ka occurring in summer. Clement et al. (2000) noted that because the most intense heating of equatorial regions occurred in the season when El Niño events begin, El Niño events should have been weak at 6 ka, and as important, greater summer warmth in the northern subtropics at 6 ka should have induced stronger easterly winds along the equator than now. Upwelling led to a cooler eastern equatorial Pacific. By contrast, Liu et al. (2000) suggested that an intensification of the South Asian monsoon, associated with greater summer insolation than today, strengthened trade winds in the tropical Pacific, which then caused a cooler eastern equatorial Pacific. Finally, Chiang et al. (2009) argued that Holocene insolation would have reduced high-latitude variability leading to reduced stochastic forcing of easterly winds in the tropics and thus to less frequent El Niño events and a cooler average eastern tropical Pacific SST. In testing which of these views might be right, Roberts et al. (2014) concluded that the question might not be unanswerable. From our perspective, however, 6-ka insolation seems to account for the cooler tropical Pacific.

A warmer Holocene Northern Hemisphere in boreal summer follows logically from the greater summer insolation at 6 ka than today. D'Agostino et al. (2019) pointed out that additional energy in the Northern Hemisphere at 6 ka requires an additional southward flux of energy to balance this enhanced difference and that most such exchange between hemispheres occurs in monsoon regions, where air with large moist static energy aloft crosses the equator from the warmer to the cooler hemisphere. Liu et al. (2017) diagnosed coupled GCM results and showed that indeed a shift in the Hadley circulation led to more heat transported southward aloft, with a coupled northward transport of heat by the ocean, which in turn moved the ITCZ northward. Thus, the North Atlantic should also have been warmer at 6 ka than today. As noted above, a strengthening of meridional heat transport across the equator should shift the EFE and the ITCZ poleward.

Paleoceanographic inferences of SSTs call for a warmer Holocene North Atlantic than today (Lohmann et al., 2013). Rimbu et al. (2003) inferred that the North Atlantic SSTs decreased from early to late Holocene and, accordingly, that the NAO indices declined over that period. This secular cooling of the North Atlantic since early Holocene is largely attributed to Northern Hemisphere cooling due to precession. Rajagopalan et al. (2019) employed the method of Gill et al. (2016) to reconstruct both the total SST and AMO signals. They estimated a warmer mid-Holocene AMO by 0.75°C.

In a comprehensive compilation of SSTs since 11,300 years ago, Marcott et al. (2013a, 2013b) showed that throughout most of the Holocene the Northern Hemisphere was warmer than in preindustrial times. We weight the estimates shown in Figure S10 of Marcott et al. (2013b) for the latitude bands of 0–30°, 30–60°, and 60–90° by 0.5, 0.37, and 0.13 to take into account different areas of each latitude band. Mean temperatures for the Northern and Southern Hemispheres at 6 ka are ~1.5°C and ~0.0°C, respectively, leading to a difference of 1.5°C. These mean temperatures apply to annual averages and therefore underestimate summer differences.

Two phenomena bear on mid-Holocene temperatures in the tropics. First, because the tropics tend to warm during El Niño events (e.g., Chiang & Sobel, 2002), with a La Niña-like mid-Holocene Pacific, the tropics

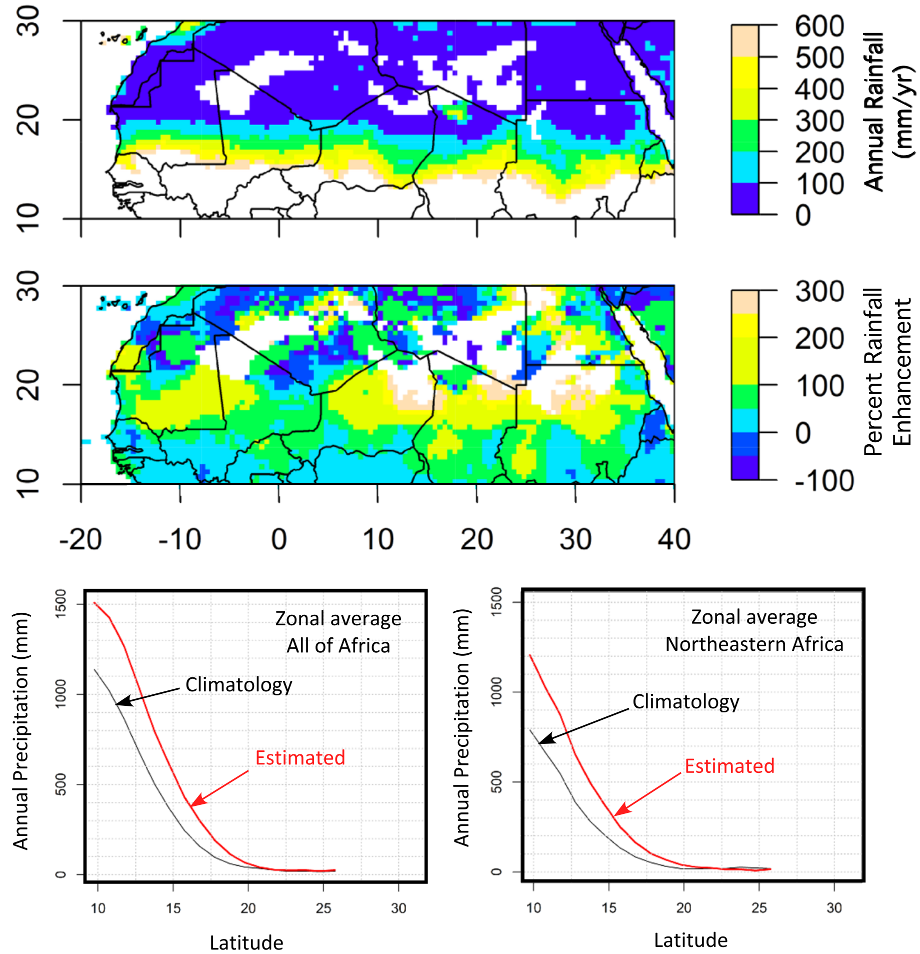

Figure 3. (top) Estimates of annual rainfall (mm/year) at ~6 ka based on local polynomial regression of historical rainfall with all four indices, (middle) percent rainfall enhancement, and (bottom) comparison of modern (black) and estimated for ~6-ka (red) annual rainfall versus latitude over North Africa (left) and northeastern Africa, 24–33°E (right).

should have been cooler than today. Adam et al. (2016a) showed that the energy flux at the equator is, indeed, lower during La Niña than El Niño. At 6 ka, summer insolation, however, was more intense near the equator than today (e.g., Adam et al., 2019), which alone would warm the equatorial band. The difference in summer insolation between the equator and the Sahel at 6 ka, however, differed little from that today (Adam et al., 2019, Figure 5b). Moreover, because of Kepler's second law, shorter summers when insolation is more intense should compensate, at least partly, for the integrated effect on equatorial temperatures (e.g., Huybers, 2006). Thus, for Holocene time, we set the coefficient for equatorial temperatures and thus, the energy flux at the equator, to that at present (no Holocene anomaly).

Using mid-Holocene values for the four indices in the local polynomial regression, we estimated Sahel-Sahara rainfall amounts and percentage deviations from the present along with latitudinal averages (Figure 3). Calculated mid-Holocene rainfall between 10°N and 22°N over the entire Sahel region exceeds that today, with a percentage difference of 50–300% between 15°N and 20°N—the core Sahel-Sahara region, and smaller south of 15°N. Compared with present-day climatology (Figure 1), rain bands covering 100 to 600 mm/year are shifted northward during mid-Holocene time, with the conspicuous shift seen in the 100- to 200-mm/year rain band from 17–18°N to ~20°N, a northward shift of ~2.5°. We computed rainfall averages for each latitude during the present day and mid-Holocene (Figure 3). Calculated mid-Holocene rainfall rates at latitudes of 15°N, 17.5°N, and 20°N exceed those today by ~250, 100, and 20 mm/year. We also computed the latitudinal average for the northeastern Africa region covering the longitudes of 24–33°E, to address the paleolakes and depressions in this region—West Nubian paleolakes, Oyo depression, and Salima Oasis. At latitudes of 15°N, 17.5°N, and 20°N in this region, calculated rainfall amounts are ~150, 50, and 20 mm/year greater than those today. Although these shifts in rainfall fall short of the paleoevidence, the shifts are more than half the range implied by paleoclimate observations summarized above.

6. Summary and Conclusions

Each of a cooler eastern tropical Pacific, a warmer North Atlantic, and a larger difference in SSTs between the northern and summer hemispheres correlates with more rainfall today over the northern edge of the Sahel. We combine estimates of Nino3.4 and AMO indices and the hemispheric SST difference for mid-Holocene time with a nonlinear local polynomial regressions to quantify the teleconnections of these indices to rainfall over Africa between 10°N and 30°N. Calculated latitudes where present-day rainfall averages 1,000, 500, or 200 mm/year lie ~2.5° farther north, and calculated mid-Holocene rainfall at 15°N, 17.5°N, and 20°N exceeds that today by 250, 100, and 20 mm/year. These shifts cannot account for estimates of mid-Holocene rainfall but are comparable with GCM runs that come closest to matching paleorainfall estimates (e.g., Braconnot et al., 2000, 2007a; Dallmeyer et al., 2015). Thus, mid-Holocene insolation seems to have altered surface temperatures that, collectively, teleconnected to rainfall over the Sahel. Although this analysis is not a diagnosis of how interconnected dynamics link Holocene insolation to surface temperatures and then to precipitation, by analogy with the blind men describing an elephant, each of the separate elements of the elephant—tropical Pacific, North Atlantic, and hemispheric difference—responds in its own way to 6-ka insolation, so that they work together to enhance rainfall over the Sahel.

Data Availability Statement

Data used in this study are available through Harris et al. (2014), Morice et al. (2012), and Kaplan et al. (1998).

Acknowledgments
We thank Emily Gill, Jody Wycech, and Yochanan Kushnir for help with estimates of the forcings during mid-Holocene. Partial support from the Crafoord Foundation is thankfully acknowledged. We thank two anonymous reviewers for constructive criticism of the manuscript.

References

Abell, P. I., & Hoelzmann, P. (2000). Holocene palaeoclimates in northwestern Sudan: Stable isotope studies on mollusks. *Global and Planetary Change*, *26*(1-3), 1–12. https://doi.org/10.1016/S0921-8181(00)00030-8

Adam, O., Bischoff, T., & Schneider, T. (2016a). Seasonal and interannual variations of the energy flux equator and ITCZ. Part I: Zonally averaged ITCZ position. *Journal of Climate*, *29*, 3219–3230.

Adam, O., Bischoff, T., & Schneider, T. (2016b). Seasonal and interannual variations of the energy flux equator and ITCZ. Part II: Zonally varying shifts of the ITCZ. *Journal of Climate*, *29*(20), 7281–7293. https://doi.org/10.1175/JCLI-D-15-0710.1

Adam, O., Schneider, T., & Brient, F. (2018). Regional and seasonal variations of the double-ITCZ bias in CMIP5 models. *Climate Dynamics*, *51*, 101–117. https://doi.org/10.1007/s00382-017-3909-1

Adam, O., Schneider, T., Enzel, Y., & Quade, J. (2019). Both differential and equatorial heating contributed to African monsoon variations during the mid-Holocene. *Earth and Planetary Science Letters*, *522*, 20–29.

Alder, J. R., & Hostetler, S. W. (2015). Global climate simulations at 3000-year intervals for the last 21 000 years with the GENMOM coupled atmosphere-ocean model. *Climate of the Past*, *11*, 449–471.

Biasutti, M., & Giannini, A. (2006). Robust Sahel drying in response to late 20th century forcings. *Geophysical Research Letters*, *33*, L11706. https://doi.org/10.1029/2006GL026067

Biasutti, M., Held, I. M., Sobel, A. H., & Giannini, A. (2008). SST forcings and Sahel rainfall variability in simulations of the twentieth and twenty-first centuries. *Journal of Climate*, *21*(14), 3471–3486. https://doi.org/10.1175/2007JCLI1896.1

Bischoff, T., & Schneider, T. (2014). Energetic constraints on the position of the Intertropical Convergence Zone. *Journal of Climate*, *27*(13), 4937–4951. https://doi.org/10.1175/JCLI-D-13-00650.1

Bischoff, T., & Schneider, T. (2016). The equatorial energy balance, ITCZ position, and double-ITCZ bifurcations. *Journal of Climate*, *29*, 2997–3013.

Bonfils, C., de Noblet-Ducoudré, N., Braconnot, P., & Joussaume, S. (2001). Hot desert albedo and climate change: Mid-Holocene monsoon in North Africa. *Journal of Climate*, *14*(17), 3724–3737. https://doi.org/10.1175/1520-0442(2001)014%3C3724:HDAACC%3E2.0.CO;2

Boos, W. R., & Korty, R. L. (2016). Regional energy budget control of the intertropical convergence zone and application to mid-Holocene rainfall. *Nature Geoscience*, *9*(12), 892–897. https://doi.org/10.1038/ngeo2833

Bosmans, J. H. C., Drijfhout, S. S., Tuenter, E., Lourens, L. J., Hilgen, F. J., & Weber, S. L. (2012). Monsoonal response to mid-holocene orbital forcing in a high resolution GCM. *Climate of the Past*, *8*, 2023–2042.

Braconnot, P., Harrison, S. P., Kageyama, M., Bartlein, P. J., Masson-Delmotte, V., Abe-Ouchi, A., et al. (2012). Evaluation of climate models using palaeoclimatic data. *Nature Climate Change*, *2*, 417–424.

Braconnot, P., Loutre, M.-F., Dong, B., Joussaume, S., Valdes, P., & Participating Groups, P. M. I. P. (2002). How the simulated change in monsoon at 6 ka BP is related to the simulation of the modern climate: Results from the Paleoclimate Modeling Intercomparison Project. *Climate Dynamics*, *19*, 107–121.

Braconnot, P., Marti, O., Joussaume, S., & Leclainche, Y. (2000). Ocean feedback in response to 6 kyr BP insolation. *Journal of Climate*, *13*(9), 1537–1553. https://doi.org/10.1175/1520-0442(2000)013%3C1537:OFIRTK%3E2.0.CO;2

Braconnot, P., Otto-Bliesner, B., Harrison, S., Joussaume, S., Peterchmitt, J.-Y., Abe-Ouchi, A., et al. (2007a). Results of PMIP2 coupled simulations of the Mid-Holocene and Last Glacial Maximum—Part 1: Experiments and large-scale features. *Climate of the Past*, *3*, 261–277.

Braconnot, P., Otto-Bliesner, B., Harrison, S., Joussaume, S., Peterchmitt, J.-Y., Abe-Ouchi, A., et al. (2007b). Results of PMIP2 coupled simulations of the Mid-Holocene and Last Glacial Maximum—Part 2: Feedbacks with emphasis on the location of the ITCZ and mid- and high latitudes heat budget. *Climate of the Past*, *3*, 279–296.

Braconnot, P., Zhu, D., Marti, O., & Servonnat, J. (2019). Strengths and challenges for transient Mid- to Late Holocene simulations with dynamical vegetation. *Climate of the Past*, *15*(3), 997–1024. https://doi.org/10.5194/cp-15-997-2019

Brown, J., Collins, M., Tudhope, A. W., & Toniazzo, T. (2008). Modelling mid-Holocene tropical climate and ENSO variability: Towards constraining predictions of future change with palaeo-data. *Climate Dynamics*, *30*, 19–36.

Charney, J. G. (1975). Dynamics of deserts and drought in the Sahel. *Quarterly Journal of the Royal Meteorological Society*, *101*(428), 193–202. https://doi.org/10.1002/qj.49710142802

Chiang, J. C. H., Fang, Y., & Chang, P. (2009). Pacific climate change and ENSO activity in the mid-Holocene. *Journal of Climate*, *22*(4), 923–939. https://doi.org/10.1175/2008JCLI2644.1

Chiang, J. C. H., & Friedman, A. R. (2012). Extratropical cooling, interhemispheric thermal gradients, and tropical climate change. *Annual Review of Earth and Planetary Sciences*, *40*(1), 383–412. https://doi.org/10.1146/annurev-earth-042711-105545

Chiang, J. C. H., & Sobel, A. H. (2002). Tropical tropospheric temperature variations caused by ENSO and their influence on the remote tropical climate. *Journal of Climate*, *15*(18), 2616–2631. https://doi.org/10.1175/1520-0442(2002)015%3C2616:TTTVCB%3E2.0.CO;2

Clement, A. C., Seager, R., & Cane, M. A. (2000). Suppression of El Niño during the mid-Holocene by changes in the Earth's orbit. *Paleoceanography*, *15*(6), 731–737. https://doi.org/10.1029/1999PA000466

D'Agostino, R., Bader, J., Bordoni, S., Ferreira, D., & Jungclaus, J. (2019). Northern Hemisphere monsoon response to mid-Holocene orbital forcing and greenhouse gas-induced global warming. *Geophysical Research Letters*, *46*, 1591–1601. https://doi.org/10.1029/2018GL081589

Dallmeyer, A., Claussen, M., Fischer, N., Haberkorn, K., Wagner, S., Pfeiffer, M., et al. (2015). The evolution of sub-monsoon systems in the Afro-Asian monsoon region during the Holocene—Comparison of different transient climate model simulations. *Climate of the Past*, *11*, 305–326.

Dallmeyer, A., Claussen, M., Lorenz, S. J., & Shanahan, T. (2018). The end of the African humid period as seen by a transient comprehensive Earth system model simulation of the last 8000 years. *Climate of the Past*, *16*, 117–140. https://doi.org/10.5194/cp-16-117-2020

de Noblet, N., Braconnot, P., Joussaume, S., & Masson, V. (1996). Sensitivity of simulated Asian and African summer monsoons to orbitally induced variations in insolation 126, 115 and 6 kBP. *Climate Dynamics*, *12*(9), 589–603. https://doi.org/10.1007/BF00216268

Donohoe, A., Marshall, J., Ferreira, D., & McGee, D. (2013). The relationship between ITCZ location and cross-equatorial atmospheric heat transport: From the seasonal cycle to the Last Glacial Maximum. *Journal of Climate*, *26*(11), 3597–3618. https://doi.org/10.1175/JCLI-D-12-00467.1

Enfield, D., Mestas-Nunez, A. M., & Trimble, P. (2001). The Atlantic multidecadal oscillation and its relation to rainfall and river flows in the continental U. S. *Geophysical Research Letters*, *28*(10), 2077–2080.

Folland, C. K., Palmer, T. N., & Parker, D. E. (1986). Sahel rainfall and worldwide sea temperatures, 1901–85. *Nature*, *320*(6063), 602–607. https://doi.org/10.1038/320602a0

Gasse, F., & Roberts, C. N. (2005). Late Quaternary hydrologic changes in the arid and semiarid belt of northern Africa. In H. F. Diaz, & R. S. Bradley (Eds.), *The Hadley circulation: Present, past and future* (pp. 313–345). Amsterdam, The Netherlands: Kluwer Academic Publishers.

Gasse, F., & Van Campo, E. (1994). Abrupt post-glacial climate events in West Africa and North Africa monsoon domains. *Earth and Planetary Science Letters*, *126*, 435–456.

Giannini, A., Biasutti, M., Held, I. M., & Sobel, A. H. (2008). A global perspective on African climate. *Climatic Change*, *90*(4), 359–383. https://doi.org/10.1007/s10584-008-9396-y

Giannini, A., Salack, S., Lodoun, T., Ali, A., Gaye, A. T., & Ndiaye, O. (2013). A unifying view of climate change in the Sahel linking intra-seasonal, interannual and longer time scales. *Environmental Research Letters*, *8*(2), 024010. https://doi.org/10.1088/1748-9326/8/2/024010

Giannini, A., Saravanan, R., & Chang, P. (2003). Oceanic forcing of Sahel rainfall on interannual to interdecadal time scales. *Science*, *302*(5647), 1027–1030. https://doi.org/10.1126/science.1089357

Gill, E. C., Rajagopalan, B., Molnar, P., & Marchitto, T. M. (2016). Reduced-dimension reconstruction of the equatorial Pacific SST and zonal wind fields over the past 10,000 years using Mg/Ca and alkenone records. *Paleoceanography*, *31*, 928–952. https://doi.org/10.1002/2016PA002948

Green, B., & Marshall, J. (2017). Coupling of trade winds with ocean circulation damps ITCZ shifts. *Journal of Climate*, *30*(12), 4395–4411. https://doi.org/10.1175/JCLI-D-16-0818.1

Green, B., Marshall, J., & Campin, J.-M. (2019). The 'sticky' ITCZ: Ocean-moderated ITCZ shifts. *Climate Dynamics*, *53*(1-2), 1–19. https://doi.org/10.1007/s00382-019-04623-5

Green, B., Marshall, J., & Donohoe, A. (2017). Twentieth century correlations between extratropical SST variability and ITCZ shifts. *Geophysical Research Letters*, *44*, 9039–9047. https://doi.org/10.1002/2017GL075044

Harris, I., Jones, P. D., Osborn, T. J., & Lister, D. H. (2014). Updated high-resolution grids of monthly climatic observations—The CRU TS3.10 dataset. *International Journal of Climatology*, *34*(3), 623–642. https://doi.org/10.1002/joc.3711

Harrison, S. P., Bartlein, P. J., Brewer, S., Prentice, I. C., Boyd, M., Hessler, I., et al. (2014). Climate model benchmarking with glacial and mid-Holocene climates. *Climate Dynamics*, *43*(3-4), 671–688. https://doi.org/10.1007/s00382-013-1922-6

Harrison, S. P., Bartlein, P. J., Izumi, K., Li, G., Annan, J., Hargreaves, J., et al. (2015). Evaluation of CMIP5 palaeo-simulations to improve climate projections. *Nature Climate Change*, *5*(8), 735–743. https://doi.org/10.1038/nclimate2649

Harrison, S. P., Jolly, D., Laarif, F., Abe-Ouchi, A., Dong, B., Herterich, K., et al. (1998). Intercomparison of simulated global vegetation distributions in response to 6 kyr BP orbital forcing. *Journal of Climate*, *11*(11), 2721–2742. https://doi.org/10.1175/1520-0442(1998)011%3C2721:IOSGVD%3E2.0.CO;2

Haynes, C. V. Jr., Eyles, C. H., Pavlish, L. A., Ritchie, J. C., & Rybak, M. (1989). Holocene palaeoecology of the eastern Sahara; Selima Oasis. *Quaternary Science Reviews*, *8*(2), 109–136. https://doi.org/10.1016/0277-3791(89)90001-2

Hillaire-Marcel, C., Riser, J., Rognon, P., Petit-Maire, N., Rosso, J. C., & Soulié-Marsche, I. (1983). Radiocarbon chronology of Holocene hydrologic changes in northeastern Mali. *Quaternary Research*, *20*(2), 145–164. https://doi.org/10.1016/0033-5894(83)90074-1

Hoelzmann, P., Jolly, D., Harrison, S. P., Laarif, F., Bonnefille, R., & Pachur, H.-J. (1998). Mid-Holocene land-surface conditions in northern Africa and the Arabian Peninsula: A data set for the analysis of biogeophysical feedbacks in the climate system. *Global Biogeochemical Cycles*, *12*(1), 35–51. https://doi.org/10.1029/97GB02733

Hoelzmann, P., Kruse, H.-J., & Rottinger, F. (2000). Precipitation estimates for the eastern Saharan palaeomonsoon based on a water balance model of the West Nubian Palaeolake Basin. *Global and Planetary Change*, *26*(1-3), 105–120. https://doi.org/10.1016/S0921-8181(00)00038-2

Huybers, P. (2006). Early Pleistocene glacial cycles and the integrated summer insolation forcing. *Science*, *313*(5786), 508–511. https://doi.org/10.1126/science.1125249

Jolly, D., Prentice, I. C., Bonnefille, R., Ballouche, A., Bengo, M., Brenac, P., et al. (1998). Biome reconstruction from pollen and plant macrofossil data for Africa and the Arabian peninsula at 0 and 6000 years. *Journal of Biogeography*, *25*(6), 1007–1027. https://doi.org/10.1046/j.1365-2699.1998.00238.x

Joussaume, S., Taylor, K. E., Braconnot, P., Mitchell, J. F. B., Kutzbach, J. E., Harrison, S. P., et al. (1999). Monsoon changes for 6000 years ago: Results of 18 simulations from the Paleoclimate Modelling Intercomparison project (PMIP). *Geophysical Research Letters*, *26*(7), 859–862. https://doi.org/10.1029/1999GL900126

Kageyama, M., Braconnot, P., Bopp, L., Mariotti, V., Roy, T., Woillez, M., et al. (2013). Mid-Holocene and Last Glacial Maximum climate simulations with the IPSL model—Part II: Model-data comparisons. *Climate Dynamics*, *40*(9-10), 2469–2495. https://doi.org/10.1007/s00382-012-1499-5

Kang, S. M., Frierson, D. M. W., & Held, I. M. (2009). The tropical response to extratropical thermal forcing in an idealized GCM: The importance of radiative feedbacks and convective parameterization. *Journal of the Atmospheric Sciences*, *66*(9), 2812–2827. https://doi.org/10.1175/2009JAS2924.1

Kang, S. M., Held, I. M., Frierson, D. M. W., & Zhao, M. (2008). The response of the ITCZ to extratropical thermal forcing: Idealized slab-ocean experiments with a GCM. *Journal of Climate*, *21*(14), 3521–3532. https://doi.org/10.1175/2007JCLI2146.1

Kaplan, A., Cane, M., Kushnir, Y., Clement, A., Blumenthal, M., & Rajagopalan, B. (1998). Analyses of global sea surface temperature 1856–1991. *Journal of Geophysical Research*, *103*(C9), 18,567–18,589. https://doi.org/10.1029/97JC01736

Knight, J. R., Allan, R. J., Folland, C. K., Vellinga, M., & Mann, M. E. (2005). A signature of persistent natural thermohaline circulation cycles in observed climate. *Geophysical Research Letters*, *32*, L20708. https://doi.org/10.1029/2005GL024233

Koutavas, A., DeMenocal, P. B., Olive, G. C., & Lynch-Stieglitz, J. (2006). Mid-Holocene El Niño–Southern Oscillation (ENSO) attenuation revealed by individual foraminifera in eastern tropical Pacific sediments. *Geology*, *34*(12), 993–996. https://doi.org/10.1130/G22810A.1

Koutavas, A., & Sachs, J. P. (2008). Northern timing of deglaciation in the eastern equatorial Pacific from alkenone paleothermometry. *Paleoceanography*, *23*, PA4205. https://doi.org/10.1029/2008PA001593

Kröpelin, S., Verschuren, D., Lézine, A.-M., Eggermont, H., Cocquyt, C., Francus, P., et al. (2008). Climate-driven ecosystem succession in the Sahara: The past 6,000 years. *Science*, *320*(5877), 765–768. https://doi.org/10.1126/science.1154913

Kuper, R., & Kröpelin, S. (2006). Climate-controlled Holocene occupation in the Sahara: Motor of Africa's evolution. *Science*, *313*(5788), 803–807. https://doi.org/10.1126/science.1130989

Kushnir, Y., & Stein, M. (2010). North Atlantic influence on 19th-20th century rainfall in the Dead Sea watershed, teleconnections with the Sahel, and implication for Holocene climate fluctuations. *Quaternary Science Reviews*, *29*(27-28), 3843–3860. https://doi.org/10.1016/j.quascirev.2010.09.004

Kutzbach, J., Bonan, G. B., Foley, J., & Harrison, S. P. (1996). Vegetation and soil feedbacks on the response of the African monsoon to orbital forcing in the early to middle Holocene. *Nature*, *384*(6610), 623–626. https://doi.org/10.1038/384623a0

Kutzbach, J. E. (1980). Estimates of past climates at paleolake Chad, North Africa, based on a hydrological and energy-balance model. *Quaternary Research*, *14*(2), 210–223. https://doi.org/10.1016/0033-5894(80)90049-6

Kutzbach, J. E. (1981). Monsoon climate of the early Holocene: Climate experiment with Earth's orbital parameters for 9000 years ago. *Science*, *214*(4516), 59–61. https://doi.org/10.1126/science.214.4516.59

Levine, X. J., & Boos, W. R. (2017). Land surface albedo bias in climate models and its association with tropical rainfall. *Geophysical Research Letters*, *44*, 6363–6372. https://doi.org/10.1002/2017GL072510

Levis, S., Bonan, G. B., & Bonfils, C. (2004). Soil feedback drives the mid-Holocene North African monsoon northward in fully coupled CCSM2 simulations with a dynamic vegetation model. *Climate Dynamics*, *23*(7-8), 791–802. https://doi.org/10.1007/s00382-004-0477-y

Lézine, A.-M., & Casanova, J. (1989). Pollen and hydrological evidences for the interpretation of past climates in tropical West Africa during the Holocene. *Quaternary Science Reviews*, *8*(1), 45–55. https://doi.org/10.1016/0277-3791(89)90020-6

Lézine, A.-M., Zheng, W., Braconnot, P., & Krinner, G. (2011). Late Holocene plant and climate evolution at Lake Yoa, northern Chad: Pollen data and climate simulations. *Climate of the Past*, *7*(4), 1351–1362. https://doi.org/10.5194/cp-7-1351-2011

Liu, X.-J., Battisti, D. S., & Donohoe, A. (2017). Tropical precipitation and cross-equatorial ocean heat transport during the Mid-Holocene. *Journal of Climate*, *11*, 3529–3547.

Liu, Y.-W., Chiang, J. C. H., Chou, C., & Patricola, C. M. (2014). Atmospheric teleconnection mechanisms of extratropical North Atlantic SST influence on Sahel rainfall. *Climate Dynamics*, *43*(9-10), 2797–2811. https://doi.org/10.1007/s00382-014-2094-8

Liu, Z.-Y., Kutzbach, J., & Wu, L.-X. (2000). Modeling climate shift of El Nino variability in the Holocene. *Geophysical Research Letters*, *27*(15), 2265–2268. https://doi.org/10.1029/2000GL011452

Loader, C. (1999). *Local regression and likelihood*. New York: Springer-Verlag.

Lohmann, G., Pfeiffer, M., Laepple, T., Leduc, G., & Kim, J.-H. (2013). A model-data comparison of the Holocene global sea surface temperature evolution. *Climate of the Past*, *9*, 1807–1839.

Lu, J., & Delworth, T. L. (2005). Oceanic forcing of the late 20th century Sahel drought. *Geophysical Research Letters*, *32*, L22706. https://doi.org/10.1029/2005GL023316

Marcott, S. A., Shakun, J. D., Clark, P. U., & Mix, A. C. (2013a). A reconstruction of regional and global temperature for the past 11,300 years. *Science*, *339*(6124), 1198–1201. https://doi.org/10.1126/science.1228026

Marcott, S. A., Shakun, J. D., Clark, P. U., & Mix, A. C. (2013b). Supplementary materials for A reconstruction of regional and global temperature for the past 11,300 years. https://www.sciencemag.org/cgi/content/full/339/6124/1198/DC1

Marshall, J., Donohoe, A., Ferreira, D., & McGee, D. (2014). The ocean's role in setting the mean position of the Inter-Tropical Convergence Zone. *Climate Dynamics*, *42*(7-8), 1967–1979. https://doi.org/10.1007/s00382-013-1767-z

Martin, E. R., Thorncroft, C., & Booth, B. B. B. (2014). The multidecadal Atlantic SST—Sahel rainfall teleconnection in CMIP5 simulations. *Journal of Climate*, *27*(2), 784–806. https://doi.org/10.1175/JCLI-D-13-00242.1

Marzin, C., & Braconnot, P. (2009). Variations of Indian and African monsoons induced by insolation changes at 6 and 9.5 kyr BP. *Climate Dynamics*, *33*(2-3), 215–231. https://doi.org/10.1007/s00382-009-0538-3

Marzin, C., Braconnot, P., & Kageyama, M. (2013). Relative impacts of insolation changes, meltwater fluxes and ice sheets on African and Asian monsoons during the Holocene. *Climate Dynamics*, *41*(9-10), 2267–2286. https://doi.org/10.1007/s00382-013-1948-9

McGee, D., & deMenocal, P. B. (2017). Climatic changes and cultural responses during the African humid period recorded in multi-proxy data. In *Oxford research encyclopedia of climate science*, New York, NY: Oxford University Press. https://doi.org/10.1093/acrefore/9780190228620.013.529

McGee, D., Donohoe, A., Marshall, J., & Ferreira, D. (2014). Changes in ITCZ location and cross-equatorial heat transport at the Last Glacial Maximum, Heinrich Stadial 1, and the mid-Holocene. *Earth and Planetary Science Letters*, *390*, 69–79. https://doi.org/10.1016/j.epsl.2013.12.043

Mees, F., Verschuren, D., Nijs, R., & Dumont, H. (1991). Holocene evolution of the crater lake at Malha, Northwest Sudan. *Journal of Paleolimnology*, *5*, 227–253.

Morice, C. P., Kennedy, J. J., Rayner, N. A., & Jones, P. D. (2012). Quantifying uncertainties in global and regional temperature change using an ensemble of observational estimates: The HadCRUT4 data set. *Journal of Geophysical Research*, *117*, D08101. https://doi.org/10.1029/2011JD017187

Otto, J., Raddatz, T., & Claussen, M. (2009). Climate variability-induced uncertainty in mid-Holocene atmosphere-ocean-vegetation feedbacks. *Geophysical Research Letters*, *36*, L23710. https://doi.org/10.1029/2009GL041457

Otto, J., Raddatz, T., Claussen, M., Brovkin, V., & Gayler, V. (2009). Separation of atmosphere-ocean-vegetation feedbacks and synergies for mid-Holocene climate. *Geophysical Research Letters*, *36*, L09701. https://doi.org/10.1029/2009GL037482

Otto-Bliesner, B. L., Brady, E. C., Clauzet, G., Tomas, R., Levis, S., & Kothavala, Z. (2006). Last Glacial Maximum and Holocene climate in CCSM3. *Journal of Climate*, *19*(11), 2526–2544. https://doi.org/10.1175/JCLI3748.1

Pachur, H.-J., & Hoelzmann, P. (1991). Paleoclimatic implications of late Quaternary lacustrine sediments in western Nubia, Sudan. *Quaternary Research*, *36*(3), 257–276. https://doi.org/10.1016/0033-5894(91)90002-M

Pachur, H.-J., & Kröpelin, S. (1987). Wadi Howar: Paleoclimatic evidence from an extinct river system in the Southeastern Sahara. *Science*, *237*(4812), 298–300. https://doi.org/10.1126/science.237.4812.298

Parhi, P., Giannini, A., Gentine, P., & Lall, U. (2016). Resolving contrasting regional rainfall responses to El Niño over tropical Africa. *Journal of Climate*, *29*(4), 1461–1476. https://doi.org/10.1175/JCLI-D-15-0071.1

Pausata, F. S. R., Messori, G., & Zhang, Q. (2016). Impacts of dust reduction on the northward expansion of the African monsoon during the Green Sahara period. *Earth and Planetary Science Letters*, *434*, 298–307.

Peings, Y., & Magnusdottir, G. (2015). Role of sea surface temperature, Arctic sea ice and Siberian snow in forcing the atmospheric circulation in winter of 2012–2013. *Climate Dynamics*, *45*(5-6), 1181–1206. https://doi.org/10.1007/s00382-014-2368-1

Perez-Sanz, A., Li, G., González-Sampériz, P., & Harrison, S. P. (2014). Evaluation of modern and mid-Holocene seasonal precipitation of the Mediterranean and northern Africa in the CMIP5 simulations. *Climate of the Past*, *10*(2), 551–568. https://doi.org/10.5194/cp-10-551-2014

Petit-Maire, N., & Riser, J. (1981). Holocene lake deposits and palaeoenvironments in central Sahara, Northeastern Mali. *Palaeogeography Palaeoclimatology Palaeoecology*, *35*, 45–61. https://doi.org/10.1016/0031-0182(81)90093-6

Peyron, O., Jolly, D., Braconnot, P., Bonnefille, R., Guiot, J., Wirrmann, D., & Chalié, F. (2006). Quantitative reconstructions of annual rainfall in Africa 6000 years ago: Model-data comparison. *Journal of Geophysical Research*, *111*, D24110. https://doi.org/10.1029/2006JD007396

Pomposi, C., Giannini, A., Kushnir, Y., & Lee, D. E. (2016). Understanding Pacific Ocean influence on interannual precipitation variability in the Sahel. *Geophysical Research Letters*, *43*, 9234–9242. https://doi.org/10.1002/2016GL069980

Pomposi, C., Kushnir, Y., Giannini, A., & Biasutti, M. (2020). Toward understanding the occurrence of both wet and dry Sahel seasons during El Niño: The modulating role of the global ocean. *Journal of Climate*, *33*(4), 1193–1207. https://doi.org/10.1175/JCLI-D-19-0219.1

Quade, J., Dente, E., Armon, M., Dor, Y. B., Morin, E., Adam, O., & Enzel, Y. (2018). Megalakes in the Sahara? A review. *Quaternary Research*, *90*(2), 253–275.

Rajagopalan, B., Gill, E., Kushnir, Y., & Wycech, J. (2019). Reduced space reconstruction of Atlantic sea surface temperature variability during Holocene from marine proxies, abstract #GC14A-05 Paper presented at AGU Fall Meeting, San Francisco, CA.

Rajagopalan, B., Kushnir, Y., & Tourre, Y. M. (1998). Observed decadal midlatitude and tropical Atlantic climate variability. *Geophysical Research Letters*, *25*(21), 3967–3970. https://doi.org/10.1029/1998GL900065

Rimbu, N., Lohmann, G., Kim, J.-H., Arz, H. W., & Schneider, R. (2003). Arctic/North Atlantic Oscillation signature in Holocene sea surface temperature trends as obtained from alkenone data. *Geophysical Research Letters*, *30*(6), 1280. https://doi.org/10.1029/2002GL016570

Ritchie, J. C., Eyles, C. H., & Haynes, C. V. (1985). Sediment and pollen evidence for an early to mid-Holocene humid period in the eastern Sahara. *Nature*, *314*(6009), 352–355. https://doi.org/10.1038/314352a0

Ritchie, J. C., & Haynes, C. V. (1987). Holocene vegetation zonation in the eastern Sahara. *Nature*, *330*(6149), 645–647. https://doi.org/10.1038/330645a0

Roberts, W. H. G., Battisti, D. S., & Tudhope, A. W. (2014). ENSO in the Mid-Holocene according to CSM and HadCM3. *Journal of Climate*, *27*(3), 1223–1242. https://doi.org/10.1175/JCLI-D-13-00251.1

Saint-Lu, M., Braconnot, P., Leloup, J., & Marti, O. (2019). The role of El Niño in the global energy redistribution: A case study in the mid-Holocene. *Climate Dynamics*, *52*(12), 7135–7152. https://doi.org/10.1007/s00382-016-3266-5

Schneider, T., Bischoff, T., & Haug, G. H. (2014). Migrations and dynamics of the intertropical convergence zone. *Nature*, *513*(7516), 45–53. https://doi.org/10.1038/nature13636

Shin, S.-I., Sardeshmukh, P. D., Webb, R. S., Oglesby, R. J., & Barsugli, J. J. (2006). Understanding the mid-Holocene climate. *Journal of Climate*, *19*(12), 2801–2817. https://doi.org/10.1175/JCLI3733.1

Street, F. A., & Grove, A. T. (1976). Environmental and climatic implications of late Quaternary lake-level fluctuations in Africa. *Nature*, *261*(5559), 385–390. https://doi.org/10.1038/261385a0

Su, H., & Neelin, J. D. (2005). Dynamical mechanisms for African monsoon changes during the mid-Holocene. *Journal of Geophysical Research*, *110*, D19105. https://doi.org/10.1029/2005JD005806

Sutton, R. T., & Hodson, D. L. (2005). Atlantic Ocean forcing of North American and European summer climate. *Science*, *309*(5731), 115–118. https://doi.org/10.1126/science.1109496

Swann, A. L. S., Fung, I. Y., Liu, Y.-w., & Chiang, J. C. H. (2014). Remote vegetation feedbacks and the Mid-Holocene green Sahara. *Journal of Climate*, *27*(13), 4857–4870. https://doi.org/10.1175/JCLI-D-13-00690.1

Tierney, J. E., Pausata, F. S. R., & deMenocal, P. B. (2017). Rainfall regimes of the green Sahara. *Science Advances*, *3*(1), e1601503. https://doi.org/10.1126/sciadv.1601503

Trenberth, K. E., & Shea, D. J. (2006). Atlantic hurricanes and natural variability in 2005. *Geophysical Research Letters*, *33*, L12704. https://doi.org/10.1029/2006GL026894

Zhang, R., & Delworth, T. L. (2006). Impact of Atlantic multidecadal oscillations on India/Sahel rainfall and Atlantic hurricanes. *Geophysical Research Letters*, *33*, L17712. https://doi.org/10.1029/2006GL026267